Two-Dimensional Graphene Bridges Enhanced Photoinduced Charge Transport in Dye-Sensitized Solar Cells

Nailiang Yang,[†,‡] Jin Zhai,[†,§,*] Dan Wang,[‡,*] Yongsheng Chen,[∥] and Lei Jiang[§]

[†]Beijing University of Aeronautics and Astronautics, Beijing 100191, People's Republic of China, [‡]State Key Laboratory of Multi-phase Complex Systems, Institute of Process Engineering, Chinese Academy of Sciences, Beijing 100190, People's Republic of China, [§]Beijing National Laboratory for Molecular Sciences (BNLMS), Center for Molecular Science, Institute of Chemistry, Chinese Academy of Sciences, Beijing 100190, People's Republic of China, and [∥]Institute of Polymer Chemistry, College of Chemistry, Nankai University, Tianjin 300071, People's Republic of China

ABSTRACT As a novel two-dimensional (2D) material, graphene shows great benefits in electric and material science. Compared to 1D nanomaterials, it may show more excellent properties. Here, we introduced graphene as 2D bridges into the nanocrystalline electrodes of dye-sensitized solar cells, which brought a faster electron transport and a lower recombination, together with a higher light scattering. On the basis of these advantages, the short-circuit current density was increased by 45% without sacrificing the open-circuit voltage, and the total conversion efficiency was 6.97%, which was increased by 39%, comparing with the nanocrystalline titanium dioxide photoanode, and it was also much better than the 1D nanomaterial composite electrode.

KEYWORDS: two-dimensional · graphene · photoanode · dye-sensitized solar cells · charge transport

Graphene, the 2D carbon nanomaterial, has drawn much attention nowadays. It is a zero band gap material,[1] and electrons in it are just like massless relativistic particles, so it has an excellent electrical conduction in two dimensions,[2−6] even at temperatures close to absolute zero and the Dirac point.[1] On the basis of its astonishing advantages in electrics, graphene has been used in conductive glasses,[7] organic photovoltaic cells,[8,9] field-effect transistor devices,[10] and ultrasensitive sensors.[11,12]

Dye-sensitized solar cells (DSSCs) have attracted considerable interests because of their relatively low cost and high efficiency for the photoelectrical conversion of solar cells since Grätzel's group introduced nanostructured TiO_2 film into anode electrodes.[13] Although ~11% conversion efficiency was obtained,[14,15] further improvements are still necessary. The major bottleneck is the transport of photogenerated electrons across the TiO_2 nanoparticle network, which competes with the charge recombination. To suppress the recombination and improve the transport, there are several strategies including (1) using composite metal oxides as the semiconductor with different band gaps,[16] (2) preparing the porous structure whose direction is perpendicular to the conducting substrate,[17−22] and (3) introducing charge carriers (1D nanomaterials) to direct photogenerated electron.[23−25]

Considering their special charge transfer properties, the 1D nanomaterials, such as the carbon nanotubes (CNTs), were introduced into the electrodes.[23−25] However, the efficiency was increased limitedly because of the point contact between nanosphere TiO_2 and columniform 1D nanomaterials (as shown in Scheme 1a). On the contrary, the 2D graphene may benefit the charge separation due to not only its excellent conductivity but also its good contact with TiO_2 nanoparticles. Graphene is a 2D soft single molecular layered structure, and there are intermolecular forces such as physisorption, electrostatic binding, or charge transfer interactions between graphene and TiO_2,[26] so the nanocrystalline TiO_2 can anchor on the graphene flake compactly (Scheme 1b) to form graphene bridges, which will decrease the TiO_2−TiO_2 contacts. Due to its excellent electrical conduction, the bridged graphene behaves as an electron transfer medium to enhance the electron transport from the conduction band (CB) of TiO_2 at the anchor position quickly (Scheme 1d), and the recombination is reduced as a result.

Herein, we incorporate the 2D graphene into TiO_2 nanostructure photoanode to form graphene bridges in DSSCs and find that graphene can enhance the charge transport rate to prevent the charge recombination and increase the light collection efficiency, as well, so the photoelectrical conversion efficiency is improved.

*Address correspondence to zhaijin@iccas.ac.cn, danwang@home.ipe.ac.cn.

Received for review November 20, 2009 and accepted January 8, 2010.

Published online January 20, 2010. 10.1021/nn901660v

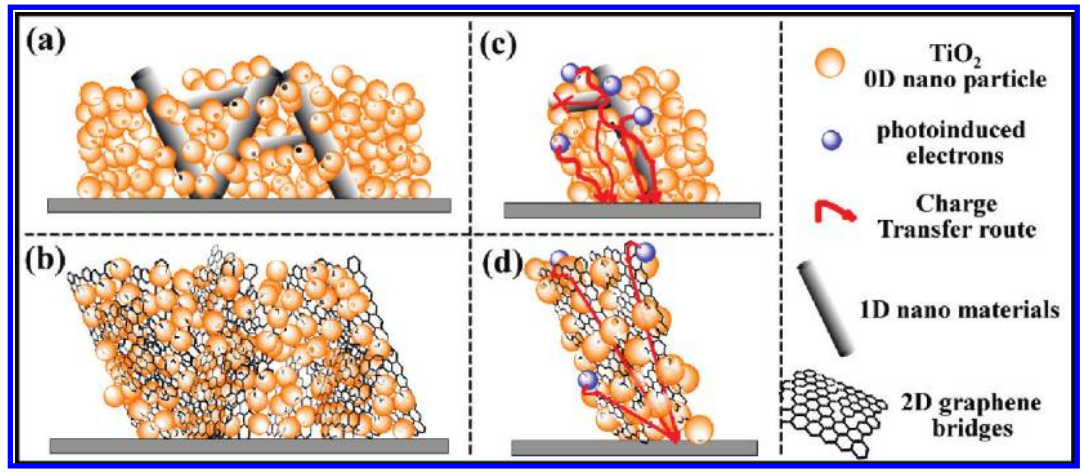

Scheme 1. Differences between (a,c) 1D and (b,d) 2D nanomaterial composite electrodes. In 2D nanomaterial composite electrodes (graphene bridges), the TiO_2 particles can anchor in the graphene better, and the photoinduced electrons can be captured and transferred by the graphene; however, with the 1D nanomaterial compositing, there are less intermolecular forces and connection between TiO_2 and the 1D nanomaterial; therefore, the transfer barrier is larger and the recombination is much easier to happen.

RESULTS AND DISCUSSION

Characterization of GO and Graphene: GO was synthesized from flake graphite by a modified Hummers method, and graphene was produced by chemical reducing and annealing (see Detailed Methods).[27] The image of GO was analyzed through atomic force microscopy (AFM) on new cleaved mica surface (Figure 1). It can be seen that the lateral dimensions of graphene are in the range of 0.2−2 μm and about 1 μm on average. Analysis of the AFM images in Figure 1b revealed the GO sheets with heights at 1 nm from the cross-sectional view in Figure 1c, which is somewhat larger than the interlayer spacing of GO (0.73 nm) measured by X-ray powder diffraction (XRD) (Supporting Information S1); however, similar results can also be observed in other results.[28−32] In addition, the X-ray photoelectron spectroscopy (XPS) (Supporting Information S2) and Fourier transform IR (FT-IR) (Supporting Information S3) measurements also confirm that the graphite was exfoliated into small pieces during the strong oxidation process, and the graphene was synthesized.[33]

Figure 2a,b shows XPS survey spectra of photoanodes with and without graphene. The C 1s peak of the electrode with graphene bridges is stronger than that without graphene, confirming that the graphene was successfully introduced into the photoanode.

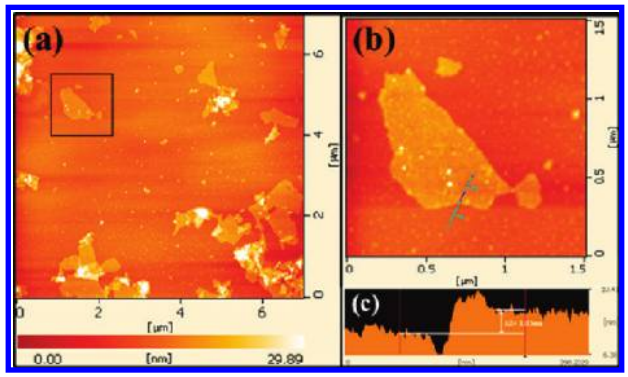

Figure 1. (a) Tapping-mode AFM image of graphene oxide. (b) Enlargement of a piece of graphene oxide. (c) Height profile through the line shown in (b).

Photocurrent−Voltage (*I*−*V*) Characteristics of Different Electrodes: In order to study the effect of 2D graphene bridges in photovoltaic devices, a series of DSSCs were fabricated with different content of graphene in the photoanode (see Detailed Methods). The traditional nanocrystalline electrode (electrode **1**) was also fabricated for comparison. The thickness of all of the different electrodes is the same (7 μm), and the results are based on the average one among many electrodes for each ratio.

The parameters and *I*−*V* characteristics for solar cells based on the different electrodes are exhibited in Table 1 and Figure 3. The results indicate that the efficiency will not be improved with the increase of the content of graphene all the while, and 0.6 wt % GO composite has the optimization (we name this electrode as electrode **2**). Considering that the GO will lose weight after the reduction, 0.4% graphene will be left in the final electrode (about 70% remaining; Supporting Information S2). Moreover, to compare the differences between the 1D and 2D composite, the CNT composite photoanode was fabricated in the same way (electrode CNT), and the content of CNT is 0.4%. Hence, electrode **1**, electrode **2**, and electrode CNT were used in the following experiments to discuss the effects of graphene.

As shown in Figure 3a, a short-circuit current density (I_{sc}) of 16.29 mA cm^{-2}, an open-circuit voltage (V_{oc}) of 0.69 V, and the conversion efficiency (η) of 6.97% for electrode **2** were obtained. As compared, an I_{sc}, V_{oc}, and η were 11.26 mA cm^{-2}, 0.69 V, and 5.01%, respectively, for electrode **1**. There is about 45% increase in I_{sc} and 39% in η for electrode **2** and nearly the same V_{oc} compared with electrode **1**. In this case, we improve the I_{sc} significantly without sacrificing the V_{oc}, indicating

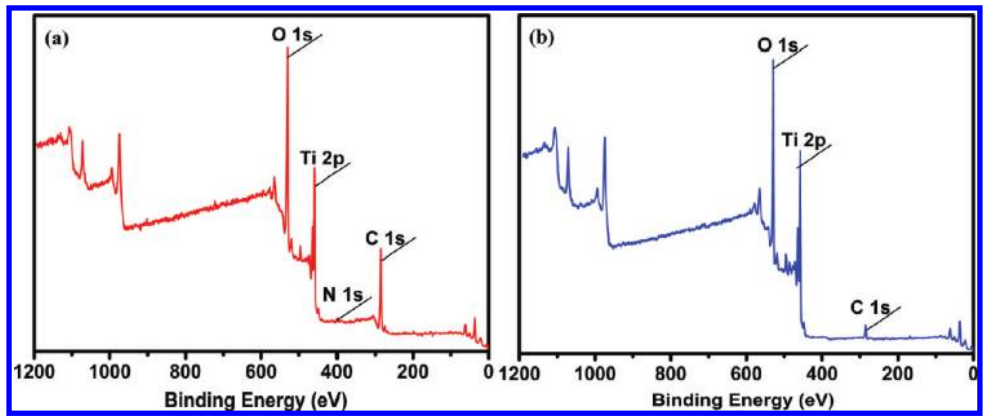

Figure 2. XPS survey spectra of the photoanode (a) with and (b) without graphene bridges.

that graphene is better than CNTs for DSSCs with the same technique.[23−25] The Fermi level of CNT is between its CB and valence band, which means it is more negative than its CB. Also, the CB of CNT is more negative (−4.5 eV *vs* vacuum) than the CB of TiO_2 (−4.0 eV *vs* vacuum). All of these make the apparent Fermi level decrease in the CNT composite cell, and the V_{oc} is sacrificed as a result.[24] However, graphene is a zero band material,[1] and its calculated work function is a little more positive (−4.42 eV *vs* vacuum) than that of CNT, which is close to work function of FTO (−4.4 eV *vs* vacuum).[7] Hence, the apparent Fermi level may not be decreased in the graphene-bridged cell, and the V_{oc} is not affected. By the way, the introduced 2D graphene bridges increase the charge transport and suppress the electrons in TiO_2 to recombine with the dye and redox species, and hence the V_{oc} will not be decreased.

Incident Monochromatic Photo-to-Current Conversion Efficiency (IPCE) Performance of Different Electrodes: In addition, the improved I_{sc} is also reflected in the increased IPCE performance (Figure 4). Compared to electrode **1**, the IPCE response at all wavelengths is enhanced by a factor of 1.56, while the maximum IPCE ($IPCE_{max}$) was 83% at the wavelength of 481 nm for electrode **2**. This increase in IPCE may be due to two factors: (1) as graphene is a 2D nanomaterial, the TiO_2 particles can anchor in it very well, so the photoinduced electrons can be captured by the graphene easily. Because graphene is an excellent electron carrier, the rapid photoinduced electron transport is produced, and the recombination and back electron transfer are suppressed as a result. (2) More porous structure of the anode has been formed due to the contributions of graphene, which increase the light scattering as shown in the SEM (Figure 5), nitrogen adsorption experiments (Figure 6a), and UV−vis spectra (Figure 6b). Furthermore, there is a blue shift to the $IPCE_{max}$. The $IPCE_{max}$ shift is common in the former reports, but the reason is not very clear.[34−36] We presume that it may be due to the introduction of many pores in the composite electrode (Figure 5b), and these pores extended the pore distribution to 500 nm (Figure 6a), which includes the wavelength around 480 nm, and the scattering more easily occurs. There is more reflectance effect around 480 nm (Figure 6b), hence the effect in IPCE is more remarkable, then the blue shift took place, and it needs further analysis.

TABLE 1. Parameters for Solar Cells Based on the Different Electrodes

GO[a] or CNT loading (wt %)	no. of electrode	V_{oc} (V)	I_{sc} (mA/cm^2)	FF (%)	η (%)
0	**1**	0.69	11.26	64.5	5.01
0.6	**2**	0.69	16.29	62.0	6.97
2.5	**3**	0.51	4.40	67.9	1.52
8.5	**4**	0.49	1.49	62.8	0.46
0.4	**CNT**	0.42	3.35	41.1	0.58

[a]The amount of GO is reduced before. It has been reduced to graphene when it was fabricated to cells. The weight loss is about 30% after the reduction.

Figure 5 shows the SEM images of the electrodes after the reduction and annealing, and there are more pores in electrode **2** (Figure 5b) than in electrode **1** (Figure 5a) and electrode CNT (Figure 5c). These pores are in the micrometer scale, and the increased pore distribution was proved by the N_2 adsorption and desorption isotherms (Figure 6a). The pore size distribution was calculated by the Barrett−Joyner−Halenda (BJH) analysis from N_2 desorption isotherms. The distribution shows that electrode **2** has large pores in the mesoporous (20−500 Å) and macroporous (>500 Å) regions. Also, the pore size was extended to the micrometer scale for the graphene composite electrode, which was formed when the H_2O and N_2H_4 were released from the anode after the reduction and annealing.[37] This means that the incorporation of graphene will introduce a hierarchical structure and increase the roughness factor, but the introduced roughness did not increase the surface area. The surface areas for electrode **1** and electrode **2** are 52.23 and 51.67 m^2 g^{-1}, respectively, calculated by the multipoint Brunauer−Emmett−Teller (BET) method, which are nearly the same, indicating that the graphene composite electrode will not improve the dye absorption, but the light scattering was increased based on the UV−vis measurement (Figure 6b). The diffuse spec-

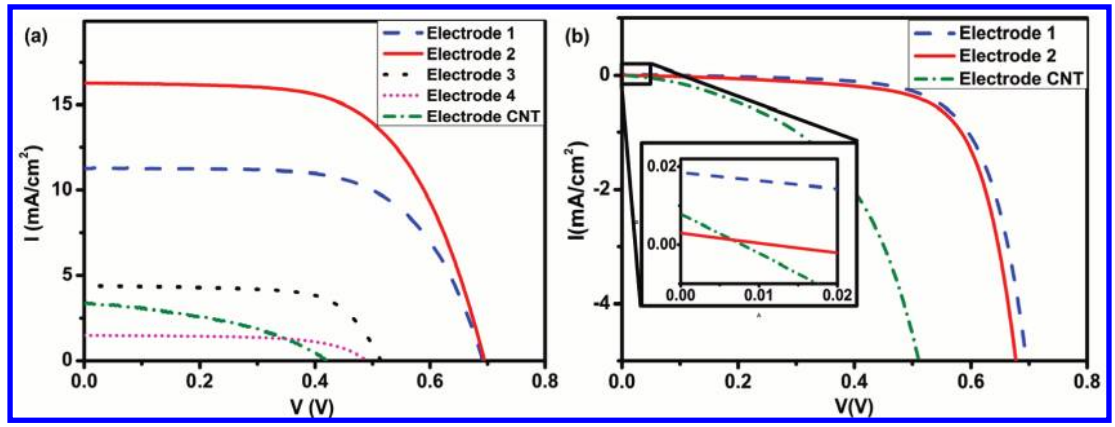

Figure 3. (a) Photocurrent−voltage characteristics of different electrodes. The sensitizer was N_3 (ruthenium dye). The cell active area was 0.20 cm^2, and the light intensity was 100 mW cm^{-2}. (b) Back-current of different electrodes (the inset of the figure is the enlarge plot of back-current).

trum shows that the introduced pore performs as a light capture center, and the light scattering was increased by 7% at all wavelengths compared to the traditional electrode. The increased light scattering will improve the photo-to-current conversion efficiency, but because the increased light diffuse cannot transform to the photoexcited electrons absolutely, the efficiency increased by light scattering must be less than 7%. However, the IPCE measurement shows the efficiency was increased by 56%. That means the major improvement is not attributed to the light scattering.

With the higher graphene loading, there will be light harvesting competition between N_3 dye and graphene, and the dye adsorption was reduced because the TiO_2 is surrounded by graphene. At the same time, the excessive graphene can act as a kind of recombination center instead of providing an electron pathway, and the short circuit will happen easily. All of these lead to the decrease of the total efficiencies.

Electrochemical Impedance Spectra (EIS) Measurement of Different Electrodes: To confirm the effect of 2D nanomaterial in transporting the electrons and restraining the recombination in the nanostructure, EIS, a powerful tool to clarify the electronic and ionic transport processes

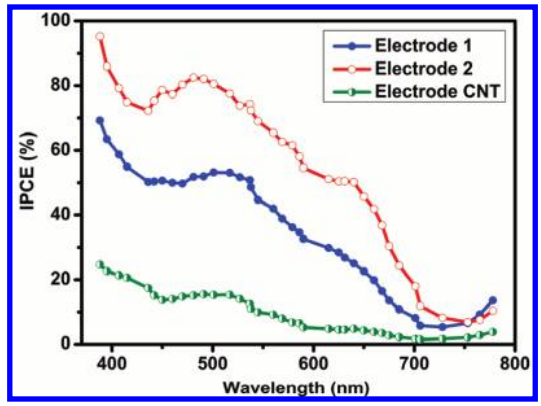

Figure 4. Photocurrent action spectra of conventional electrode (electrode 1), TiO_2−graphene composite electrode (electrode 2), and the CNT composite electrode. IPCE(%) = $(1241I_{sc})/(\lambda P_{in}) \times 100$, where I_{sc} is short-circuit current and P_{in} is the power of the incident light.

in DSSCs,[38,39] was measured under the illumination of one sun at open-circuit potential (Figure 7). In the Nyquist plots (Figure 7a), the biggest semicircle at medium frequencies is attributed to photoinjected electrons in the TiO_2 or back reaction from the injected electrons in TiO_2 to the electrolyte (*ca.* 1−100 Hz), which is the most important in the device. As shown, the semicycle at intermediate frequency regions was decreased for electrode **2**, indicating the fast redox activity of the electrolyte in the working electrode interface. The equivalent circuit of the devices (Figure 7c) has been reported.[40−42] Using Z View software and fitting the semicircle of medium frequencies gives R_3 (resistance of charge transfer) and C_1 (capacity). Compared with electrode **1**, electrode **2** has a smaller R_3 (21.66 *vs* 29.86 Ω) but a bigger C_1 (1655 *vs* 965 μF), showing that the charge recombination in electrode **2** has been reduced. These results were also supported by the Bode plots (Figure 7b). The medium frequency peak of electrode **2** is shifted to lower frequency (from ∼10.1 to ∼6.9 Hz), compared to electrode **1**. Therefore, incorporating graphene into the TiO_2 nanocrystalline anode will increase the electron transport rate to restrain the charge recombination.

In addition, some 1D nanomaterials are also good electron carriers, to prove the outstanding properties of the 2D nanomaterial, the CNT composite electrodes were also fabricated in the same route, and the surface area of electrode CNT was almost the same with other electrodes (53.08 $m^2\ g^{-1}$). As shown in the previous figures (electrode CNT), this electrode had a low efficiency (0.58%), and the IPCE was low too. The reasons were observed by the EIS measurement. Electrode CNT has the largest R_3 (140 Ω) and smallest C_1 (28 μF), and the medium frequency peak is at 107 Hz (the highest). These results indicate the CNT is not an ideal charge carrier in this system. The low dark current proves that CNT is a good electron capturer[25] (Figure 3b), and it is a good conductor indubitably. However, its performance in DSSCs is not so good. That may be due to

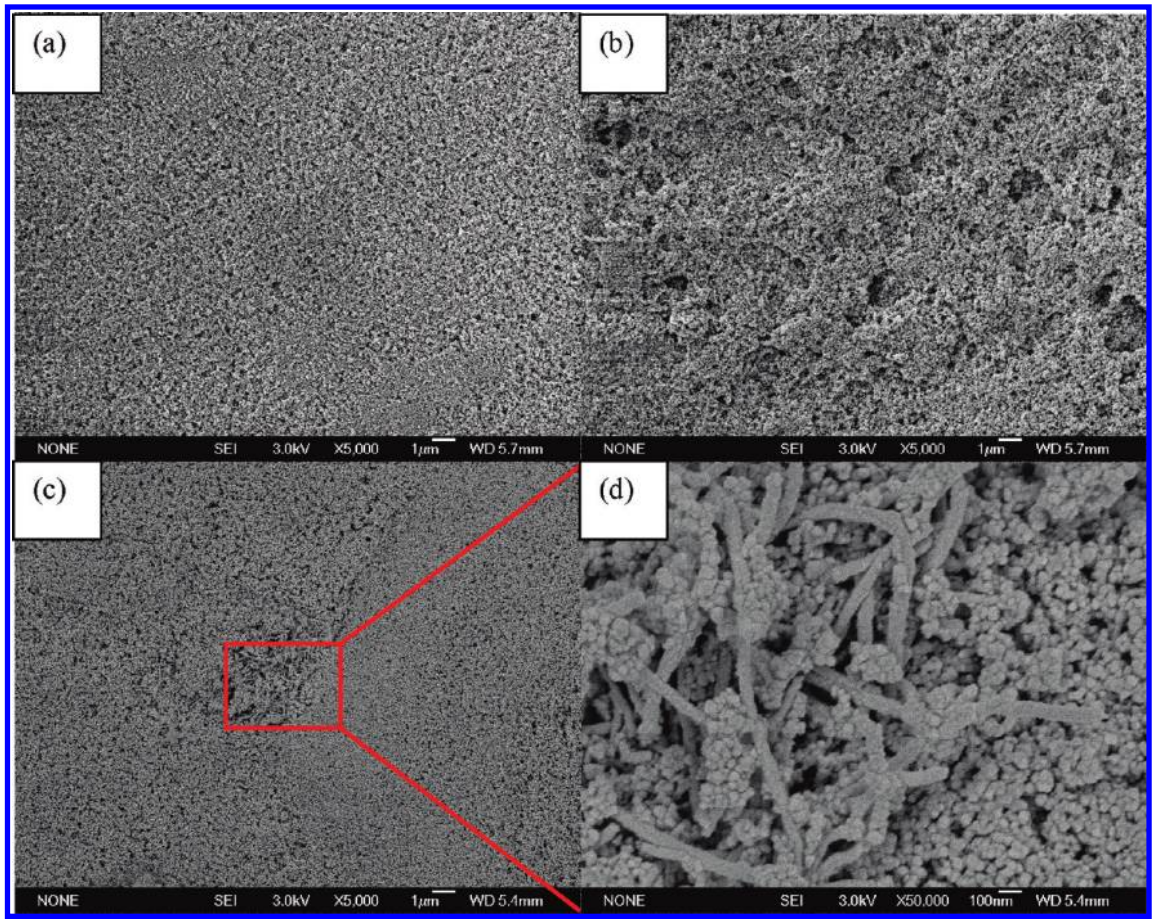

Figure 5. SEM micrographs of (a) electrode 1, (b) electrode 2, and (c,d) electrode CNT. The graphene composite electrode will be more porous compared to other electrodes. (d) Enlargement of (c). Panel d indicates that the CNT cannot connect to the TiO_2 particle well, and it is the point contact. The CNT cannot also disperse in the anode well, which may also restrict the efficiency.

two factors: (1) CNT is a 1D nanomaterial. The columniform structure cannot attach the TiO_2 particles well, and it is isolated in the anode (Figure 5d). It will not perform as the electron capturer and carrier well. (2) The CNT is not coherent, and the captured electrons cannot transport to the FTO (because the CNT is not coherent) or TiO_2 (due to the energy level reason), and the resistance is high (R_3) as a result. Also, many electrons are captured by CNT without transporting; hence the electrons are superfluous, and the recombination occurs more easily; therefore, the capacity (C_1) is low and the frequency is high. Also, in the CNT composite cell, the light scattering is the lowest, but the transmittance is the highest (Supporting Information S4), and the efficiency was decreased to some extent.

Operational Principle of the Device: Due to its excellent electrical conduction, the 2D graphene bridges behave as an electron transfer channel, which can transport the

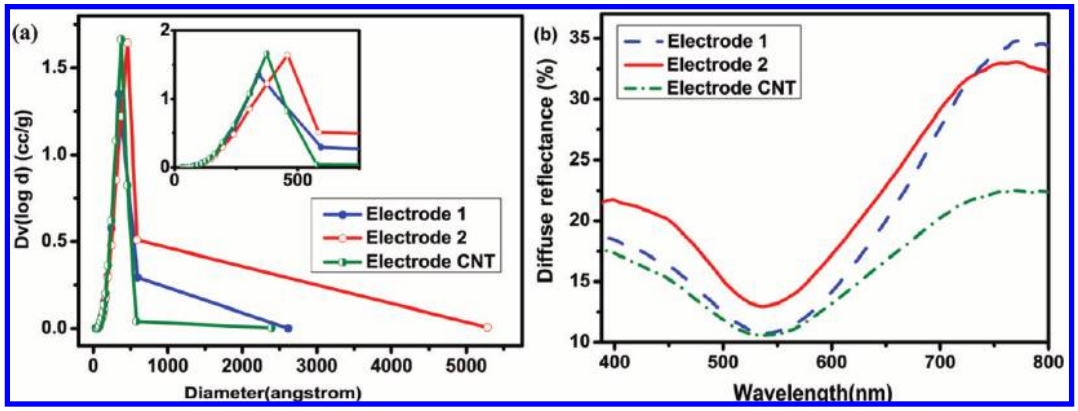

Figure 6. (a) BJH pore size distributions calculated from N_2 desorption isotherms, and (b) measured diffuse reflectance of sensitized anodes.

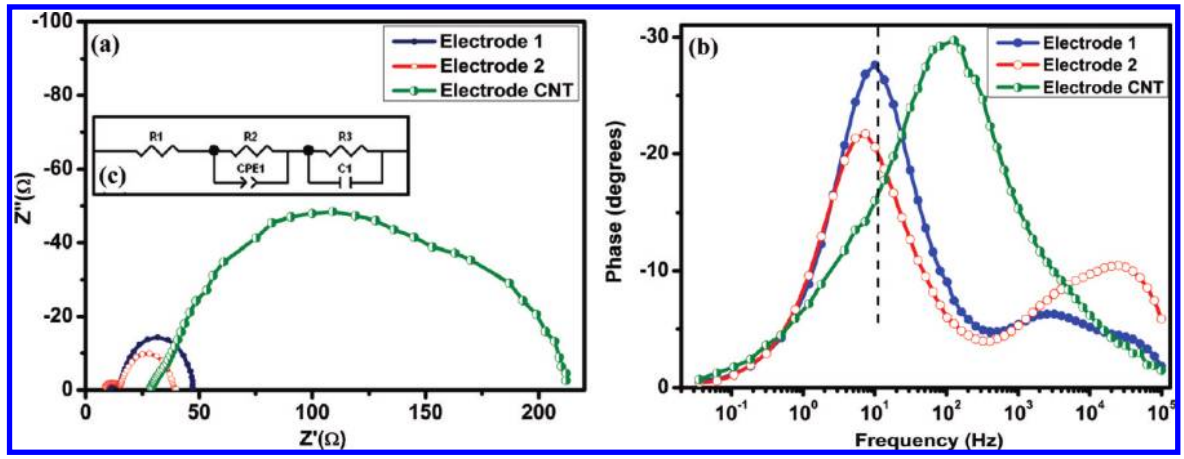

Figure 7. (a) Nyquist and (b) Bode diagrams of the electrochemical impedance spectra of different electrodes. (c) Equivalent circuit of the device. The spectra were measured under the illumination of one sun at open-circuit potential.

photoinduced electron quickly,[23] and the energy level of graphene is between the CB of TiO_2 and FTO.[43] Scheme 2 shows the operational principle. Under illumination, the CB of semiconductor TiO_2 receives the electrons from photoexcited dye. Because the TiO_2 is anchored with 2D graphene, and the graphene is homogeneous in the system, the excited electrons are captured by the graphene without any obstruction. The collected electrons can transport from TiO_2 to the conductive substrate quickly and effectively through graphene bridges (Scheme 1d), and hence the adverse reactions (recombination and back reaction) are suppressed.

CONCLUSIONS

In summary, 2D graphene is a rising star in material science, and we introduced it into the nanocrystalline anode of DSSC successfully. The short-circuit current density was increased by 45%, and the conversion efficiency was increased by 39%. This may be due to a lower recombination and a faster electron transport with the introduction of graphene chiefly. Also, the higher light scattering is a benefit to a certain extent. This study proved that the 2D charge carriers have more advantages than the 1D material, such as compactly anchoring and homogeneous dispersion. The incorporation of 2D nanomaterial with 0D nanoparticles can also be extended to other electronic devices, especially using graphene as an electron acceptor and charge transfer medium.

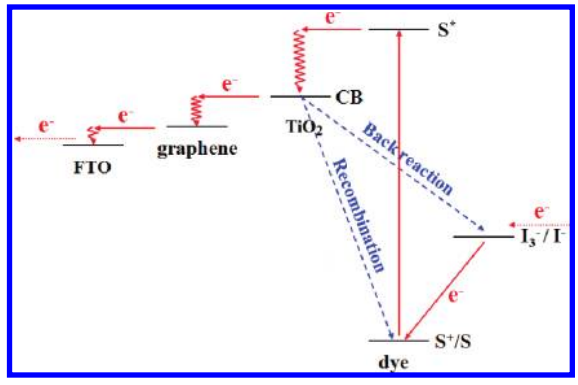

Scheme 2. Operational principle of the device: the introduced 2D graphene bridges perform as an electron acceptor and transfer the electrons quickly. Hence, the recombination and back reaction are suppressed.

DETAILED METHODS

Synthesis of GO: GO was synthesized from flake graphite (average particle diameter of 4 μm, Qingdao Tianhe Graphite Co. Ltd., Qingdao, China) by a modified Hummers method.[27] All of the other chemicals were of analytical reagent grade and used without further purification. Briefly, graphite powder (5 g) and $NaNO_3$ (3.75 g) were placed in a flask. Then, concentrated H_2SO_4 (375 mL) was added slowly with stirring in an ice−water bath. $KMnO_4$ (22.5 g) was added gradually under stirring over 1 h and kept stirring for another 2 h. After stirring vigorously for 5 days at room temperature, the mixture was stirred at 35 °C for 2 h, and then diluted with 5 wt % H_2SO_4 aqueous solution (700 mL) over 1 h. After stirring at 98 °C for 2 h, when the temperature was reduced to 60 °C, 30 wt % H_2O_2 (30 mL) was added, and the mixture was stirred for 2 h at room temperature. The mixture was centrifugated and washed with aqueous solution of 3 wt % H_2SO_4/0.5 wt % H_2O_2 (2 L) 15 times. Then the bottom solid was washed with 3 wt % HCl (2 L) aqueous solution with a similar procedure and one time using H_2O (2 L). After adding another 2 L of deionized water and dispersing the solid using vigorous stirring and bath ultrasonication for 30 min, the final water solution was treated with a weak basic ion-exchange resin to remove the remaining HCl acid. The final solution was concentrated to 7.5 mg/mL.

Preparation of Different DSSCs: To prepare the graphene composite electrode, 3 g of poly(vinylalcohol) (PVA, MW 22 000) water solution (30%) was dissolved with the mixed solvent containing 9 mL of H_2O and 12.5 mL of ethanol. Then, 1.62 g of P-25 TiO_2 was added to make the suspension of TiO_2. After the suspension was dispersed, electrode **1** was prepared by doctor-blade tech-

nique on fluorine-doped tin oxide (FTO) glass for comparison. For the preparation of graphene composite electrodes, 1.25 mL of GO aqueous solution (7.5 mg/mL) was added into the suspension (0.6 wt %). After that, it was stirred and dispersed in ultrasonic cleaner for about 30 min to let GO disperse in the suspension well, and it can anchor TiO_2 perfectly; then electrode **2** was prepared. Also, the electrodes with 2.5 and 8.5 wt % content of GO were prepared (electrode **3** and **4**) in the same way. In addition, the CNT composite electrode (0.4 wt %) was fabricated as 1.62 g of P-25 TiO_2, 3 g of PVA water solution (30%), 9 mL of H_2O, 12.5 mL of ethanol, and 6.5 mg of CNT (Shenzhen Nanotech Port Co. Ltd., the diameter is 20−40 nm, and the purity is >95%), and the fabricated route is the same. The thickness of all the different films is about 7 μm. At last, the electrodes were treated under hydrazine vapor at 40 °C for 24 h to reduce GO. After the films were rinsed with deionized water and dried by heating to 40 °C in vacuum for 3 h, the electrodes were annealed at 400 °C under argon flow for 3 h, and the GO was transformed to graphene totally. Then, they were calcined at 450 °C for 1 h in air. The as-prepared films were sensitized by soaking in ethanol solution containing 3×10^{-4} M ruthenium dye, $Ru(dcbpy)_2(NCS)_2$ (N_3) (dcbpy = 2,2′-bipyridine- 4,4′-dicarboxylic acid) for 24 h. The DSSCs were composed of a sensitized photoanode, a platinum counter electrode, and an electrolyte. The electrolyte was composed of 0.5 M LiI, 0.05 M I_2, 0.5 M *tert*-butylpyridine, and 0.6 M 1-propyl-3-methylimidazolium iodide in 3-methoxypropionitrile.

Characterization: The AFM images were measured with SPA400 (Seiko Instruments Inc.) on new cleaved mica surface in tapping mode in air. The XRD patterns were obtained by using an X'Pert PRO MDP with Cu Kα radiation (λ = 1.5405 Å) with 30 mA and 40 kV. XPS data were obtained with an ESCALab220i-XL electron spectrometer from VG Scientific using 300 W Al Kα radiation. The FT-IR spectrum was recorded by a Bruker Equinox 55 FTIR spectrometer. The *I*−*V* characteristics of the cell were measured by an electrochemical analyzer (CHI630A, Chenhua Instruments Co., Shanghai) under solar simulator illumination (CMH-250, Aodite Photoelectronic Technology Ltd., Beijing) at room temperature. The IPCE was measured by illumination with monochromatic light, which was obtained by a series of light filters with different wavelengths. SEM images were obtained using a JEOL JSM-6700F scanning electron microscope at 3.0 kV. UV−vis spectra were recorded on a Hitachi Model U-4100 spectrophotometer. The nitrogen adsorption and desorption isotherms at the temperature of liquid nitrogen (77 K) were measured on a Quantachrome Autosorb-1 sorption analyzer with prior degassing under vacuum at 200 °C overnight. Total pore volumes were determined using the adsorbed volume at a relative pressure of 0.99. Multipoint BET surface area was estimated from the relative pressure range from 0.05 to 0.2. The pore size distribution of the electrodes was analyzed using the BJH algorithm. The EIS was carried out on a Zahner IM6e impedance analyzer (Germany) in the frequency range of 0.02 Hz to 100 kHz with illumination of 100 mW/cm^2.

Acknowledgment. We thank the NSFC (90306011 and 20774101), National Basic Research Program (2006CB806203, 2006CB932102, and 2007CB936403), 863 Program 2007AA03Z327 for continuing financial support.

Supporting Information Available: Detailed experimental procedures and additional figures. This material is available free of charge *via* the Internet at http://pubs.acs.org.

REFERENCES AND NOTES

1. Freitag, M. Graphene: Nanoelectronics Goes Flat Out. *Nat. Nanotechnol.* **2008**, *3*, 455–457.
2. Geim, A. K.; Novoselov, K. S. The Rise of Graphene. *Nat. Mater.* **2007**, *6*, 183–191.
3. Novoselov, K. S.; Geim, A. K.; Morozov, S. V.; Jiang, D.; Zhang, Y.; Dubonos, S. V.; Grigorieva, I. V.; Firsov, A. A. Electric Field Effect in Atomically Thin Carbon Films. *Science* **2004**, *306*, 666–669.
4. Stankovich, S.; Dikin, D. A.; Dommett, G. H. B.; Kohlhaas, K. M.; Zimney, E. J.; Stach, E. A.; Piner, R. D.; Nguyen, S. T.; Ruoff, R. S. Graphene-Based Composite Materials. *Nature* **2006**, *442*, 282–286.
5. Katsnelson, M. I. Graphene: Carbon in Two Dimensions. *Mater. Today* **2007**, *10*, 20–27.
6. Li, D.; Kaner, R. B. Materials Science: Graphene-Based Materials. *Science* **2008**, *320*, 1170–1171.
7. Wang, X.; Zhi, L.; Müllen, K. Transparent, Conductive Graphene Electrodes for Dye-Sensitized Solar Cells. *Nano Lett.* **2008**, *8*, 323–327.
8. Liu, Z. F.; Liu, Q.; Huang, Y.; Ma, Y. F.; Yin, S. G.; Zhang, X. Y.; Sun, W.; Chen, Y. S. Organic Photovoltaic Devices Based on a Novel Acceptor Material: Graphene. *Adv. Mater.* **2008**, *20*, 3924–3930.
9. Liu, Q.; Liu, Z. F.; Zhang, X. Y.; Yang, L. Y.; Zhang, N.; Pan, G. L.; Yin, S. G.; Chen, Y. S.; Wei, J. Polymer Photovoltaic Cells Based on Solution-Processable Graphene and P3HT. *Adv. Funct. Mater.* **2009**, *19*, 894–904.
10. Di, C. A.; Wei, D. C.; Yu, G.; Liu, Y. Q.; Guo, Y. L.; Zhu, D. B. Patterned Graphene as Source/Drain Electrodes for Bottom-Contact Organic Field-Effect Transistors. *Adv. Mater.* **2008**, *20*, 3289–3293.
11. Schedin, F.; Geim, A. K.; Morozov, S. V.; Hill, E. W.; Blake, P.; Katsnelson, M. I.; Novoselov, K. S. Detection of Individual Gas Molecules Adsorbed on Graphene. *Nat. Mater.* **2007**, *6*, 652–655.
12. Ang, P. K.; Chen, W.; Wee, A. T. S.; Loh, K. P. Solution-Gated Epitaxial Graphene as pH Sensor. *J. Am. Chem. Soc.* **2008**, *130*, 14392–14393.
13. O'Regan, B.; Grätzel, M. A Low-Cost, High-Efficiency Solar Cell Based on Dye-Sensitized Colloidal TiO_2 Films. *Nature* **1991**, *353*, 737–740.
14. Nazeeruddin, M. K.; De Angelis, F.; Fantacci, S.; Selloni, A.; Viscardi, G.; Liska, P.; Ito, S.; Takeru, B.; Grätzel, M. Combined Experimental and DFT-TDDFT Computational Study of Photoelectrochemical Cell Ruthenium Sensitizers. *J. Am. Chem. Soc.* **2005**, *127*, 16835–16847.
15. Chiba, Y.; Islam, A.; Watanabe, Y.; Komiya, R.; Koide, N.; Han, L. Dye-Sensitized Solar Cells with Conversion Efficiency of 11.1%. *Jpn. J. Appl. Phys.* **2006**, *45*, L638–L640.
16. Kong, F. T.; Dai, S. Y.; Wang, K. J. Review of Recent Progress in Dye-Sensitized Solar Cells. *Adv. Optoelectron.* **2007**, *2007*, 1–13.
17. Kong, F. T.; Dai, S. Y. Dye-Sensitized Solar Cells. *Prog. Chem.* **2006**, *18*, 1409–1424.
18. Kuang, D. B.; Brillet, J.; Chen, P.; Takata, M.; Uchida, S.; Miura, H.; Sumioka, K.; Zakeeruddin, S. M.; Grätzel, M.

Application of Highly Ordered TiO_2 Nanotube Arrays in Flexible Dye-Sensitized Solar Cells. *ACS Nano* **2008**, *2*, 1113–1116.
19. Mor, G. K.; Shankar, K.; Paulose, M.; Varghese, O. K.; Grimes, C. A. Use of Highly-Ordered TiO_2 Nanotube Arrays in Dye-Sensitized Solar Cells. *Nano Lett.* **2006**, *6*, 215–218.
20. Grimes, C. A. Synthesis and Application of Highly Ordered Arrays of TiO_2 Nanotubes. *J. Mater. Chem.* **2007**, *17*, 1451–1457.
21. Zhu, K.; Neale, N. R.; Miedaner, A.; Frank, A. J. Enhanced Charge-Collection Efficiencies and Light Scattering in Dye-Sensitized Solar Cells Using Oriented TiO_2 Nanotubes Arrays. *Nano Lett.* **2007**, *7*, 69–74.
22. Jennings, J. R.; Ghicov, A.; Peter, L. M.; Schmuki, P.; Walker, A. B. Dye-Sensitized Solar Cells Based on Oriented TiO_2 Nanotube Arrays: Transport, Trapping, and Transfer of Electrons. *J. Am. Chem. Soc.* **2008**, *130*, 13364–13372.
23. Kongkanand, A.; Martinez-Dominguez, R.; Kamat, P. V. Single Wall Carbon Nanotube Scaffolds for Photoelectrochemical Solar Cells. Capture and Transport of Photogenerated Electrons. *Nano Lett.* **2007**, *7*, 676–680.
24. Brown, P.; Takechi, K.; Kamat, P. V. Single-Walled Carbon Nanotube Scaffolds for Dye-Sensitized Solar Cells. *J. Phys. Chem. C* **2008**, *112*, 4776–4782.
25. Yen, C. Y.; Lin, Y. F.; Liao, S. H.; Weng, C. C.; Huang, C. C.; Hsiao, Y. H.; Ma, C. C. M.; Chang, M. C.; Shao, H.; Tsai, M. C.; *et al.* Preparation and Properties of a Carbon Nanotube-Based Nanocomposite Photoanode for Dye-Sensitized Solar Cells. *Nanotechnology* **2008**, *19*, 1–9.
26. Williams, G.; Seger, B.; Kamat, P. V. TiO_2-Graphene Nanocomposites. UV-Assisted Photocatalytic Reduction of Graphene Oxide. *ACS Nano* **2008**, *2*, 1487–1491.
27. Becerril, H. A.; Mao, J.; Liu, Z.; Stoltenberg, R. M.; Bao, Z.; Chen, Y. Evaluation of Solution-Processed Reduced Graphene Oxide Films as Transparent Conductors. *ACS Nano* **2008**, *2*, 463–470.
28. Niyogi, S.; Bekyarova, E.; Itkis, M. E.; McWilliams, J. L.; Hamon, M. A.; Haddon, R. C. Solution Properties of Graphite and Graphene. *J. Am. Chem. Soc.* **2006**, *128*, 7720–7721.
29. Xu, Y. X.; Bai, H.; Lu, G. W.; Li, C.; Shi, G. Q. Flexible Graphene Films *via* the Filtration of Water-Soluble Noncovalent Functionalized Graphene Sheets. *J. Am. Chem. Soc.* **2008**, *130*, 5856–5857.
30. Gomez-Navarro, C.; Weitz, R. T.; Bittner, A. M.; Scolari, M.; Mews, A.; Burghard, M.; Kern, K. Electronic Transport Properties of Individual Chemically Reduced Graphene Oxide Sheets. *Nano Lett.* **2007**, *7*, 3499–3503.
31. Nakashima, N.; Tomonari, Y.; Murakami, H. Water-Soluble Single-Walled Carbon Nanotubes *via* Noncovalent Sidewall-Functionalization with a Pyrene-Carrying Ammonium Ion. *Chem. Lett.* **2002**, *31*, 638–639.
32. Nakayama-Ratchford, N.; Bangsaruntip, S.; Sun, X.; Welsher, K.; Dai, H. J. Noncovalent Functionalization of Carbon Nanotubes by Fluorescein-Polyethylene Glycol: Supramolecular Conjugates with pH-Dependent Absorbance and Fluorescence. *J. Am. Chem. Soc.* **2007**, *129*, 2448–2449.
33. Nethravathi, C.; Rajamathi, M. Chemically Modified Graphene Sheets Produced by the Solvothermal Reduction of Colloidal Dispersions of Graphite Oxide. *Carbon* **2008**, *46*, 1994–1998.
34. Yum, J. H.; Hagberg, D. P.; Moon, S. J.; Karlsson, K. M.; Marinado, T.; Sun, L. C.; Hagfeldt, A.; Nazeeruddin, M. K.; Grätzel, M. A Light-Resistant Organic Sensitizer for Solar-Cell Applications. *Angew. Chem., Int. Ed.* **2009**, *48*, 1576–1580.
35. Tian, H. N.; Yang, X. C.; Chen, R. K.; Pan, Y. Z.; Li, L.; Hagfeldt, A.; Sun, L. C. Phenothiazine Derivatives for Efficient Organic Dye-Sensitized Solar Cells. *Chem. Commun.* **2007**, 3741–3743.
36. Jennings, J. R.; Ghicov, A.; Peter, L. M.; Schmuki, P.; Walker, A. B. Dye-Sensitized Solar Cells Based on Oriented TiO_2 Nanotube Arrays: Transport, Trapping, and Transfer of Electrons. *J. Am. Chem. Soc.* **2008**, *130*, 13364–13372.
37. Stankovich, S.; Dikin, D. A.; Piner, R. D.; Kohlhaas, K. A.; Kleinhammes, A.; Jia, Y.; Wu, Y.; Nguyen, S. T.; Ruoff, R. S. Synthesis of Graphene-Based Nanosheets *via* Chemical Reduction of Exfoliated Graphite Oxide. *Carbon* **2007**, *45*, 1558–1565.
38. Kubo, W.; Murakoshi, K.; Kitamura, T.; Yoshida, S.; Haruki, M.; Hanabusa, K; Shirai, H.; Wada, Y.; Yanagida, S. Quasi-Solid-State Dye-Sensitized TiO_2 Solar Cells: Effective Charge Transport in Mesoporous Space Filled with Gel Electrolytes Containing Iodide and Iodine. *J. Phys. Chem. B* **2001**, *105*, 12809–12815.
39. Zhao, Y.; Zhai, J.; Wei, T. X.; Jiang, L.; Zhu, D. B. Enhanced Photoelectrical Performance of TiO_2 Electrodes Integrated with Microtube-Network Structures. *J. Mater. Chem.* **2007**, *17*, 5084–5089.
40. Park, N. G.; Kim, K. M.; Kang, M. G.; Ryu, K. S.; Chang, S. H.; Shin, Y. J. Chemical Sintering of Nanoparticles: A Methodology for Low-Temperature Fabrication of Dye-Sensitized TiO_2 Films. *Adv. Mater.* **2005**, *17*, 2349–2353.
41. Wang, Q.; Moser, J. E.; Grätzel, M. Electrochemical Impedance Spectroscopic Analysis of Dye-Sensitized Solar Cells. *J. Phys. Chem. B* **2005**, *109*, 14945–14953.
42. van de Lagemaat, J.; Park, N. G.; Frank, A. J. Influence of Electrical Potential Distribution, Charge Transport, and Recombination on the Photopotential and Photocurrent Conversion Efficiency of Dye-Sensitized Nanocrystalline TiO_2 Solar Cells: A Study by Electrical Impedance and Optical Modulation Techniques. *J. Phys. Chem. B* **2000**, *104*, 2044–2052.
43. Grätzel, M. Photoelectrochemical Cells. *Nature* **2001**, *414*, 338–344.